Hypersonic Lifting Body Boundary-Layer Analysis at High Angles of Incidence

J. C. ADAMS JR.* AND W. R. MARTINDALE†
ARO, Inc., Arnold Air Force Station, Tenn.

Formulation and application of a windward surface boundary-layer analysis are presented for general lifting body configurations at high angles of incidence under hypersonic perfect gas conditions. The present technique applies the "strip theory" concept, leading to an infinite-extent yawed body treatment applied in the windward surface crossflow plane for both the inviscid and viscous (boundary-layer) flowfields. A one-strip integral relations approach is used to determine the spanwise surface pressure distribution at a given body location with all inviscid centerline quantities determined via an inviscid conical flow approach. The boundary-layer analysis is based on implicit finite-difference integration of the governing equations for infinite-extent, yawed, blunt-body boundary layers. Both laminar and turbulent flows are considered using a three-dimensional eddy viscosity mixing length model of turbulence. Comparisons of the present "strip theory" approach with experimental data on Space Shuttle configurations are presented. Results of the current study include the tentative identification of spanwise crossflow-induced boundary-layer transition and a $\frac{3}{10}$-power scaling of turbulent boundary-layer heat-transfer rate with respect to changes in the freestream Reynolds number as well as verification of the wall temperature effect on turbulent boundary-layer heat transfer as reflected in the Stanton number.

Nomenclature

dU_e/dx = inviscid crossflow velocity gradient
$\bar{G}$ = scalar velocity function defined by Eq. (9)
$\bar{H}$ = mean total enthalpy
H_∞ = freestream total enthalpy
$\bar{h}$ = mean static enthalpy
h_w = wall static enthalpy
k_* = inner law mixing-length constant, 0.435
L = reference length
l_* = mixing length defined by Eq. (10)
M_∞ = freestream Mach number
Pr = laminar Prandtl number, 0.71
Pr_t = turbulent Prandtl number, 0.90
$\bar{p}$ = static pressure
$p_\text{℄}$ = centerline pressure
p_∞ = freestream static pressure
$\dot{q}$ = heat flux
$\dot{q}_w$ = wall heat flux
Re_∞ = freestream unit Reynolds number, $\rho_\infty V_\infty/\mu_\infty$, (1/ft)
St_∞ = local Stanton number, $\dfrac{-\dot{q}_w}{\rho_\infty V_\infty(H_\infty - h_w)}$
$St_{\infty,\text{ref}}$ = reference Stanton number corresponding to the laminar axisymmetric stagnation point flow on a scaled 1 ft radius sphere
$T_{0,\infty}$ = freestream stagnation temperature
T_{pc} = phase-change paint temperature
T_w = wall temperature
U_e = crossflow velocity component at outer edge of boundary layer
$\bar{u}$ = mean crossflow velocity component
$\bar{u}_{sl}$ = streamwise velocity in streamline coordinates
V = combined normal velocity components
V_∞ = freestream velocity
v' = fluctuating normal velocity component
$\bar{v}$ = mean normal velocity component
W_e = streamwise velocity component at outer edge of boundary layer
$\bar{w}$ = mean streamwise velocity component
$\bar{w}_{sl,\max}$ = maximum crossflow velocity in streamline coordinates as defined in Fig. 2
x = crossflow coordinate normal to body centerline
x^* = crossflow coordinate distance from body centerline to location of sonic point
y = coordinate normal to body surface
y_l = characteristic thickness of boundary layer
z = streamwise coordinate along body centerline
α = angle of attack
β = inviscid velocity gradient parameter, $(2\xi/U_e)(dU_e/d\xi)$
δ = boundary-layer thickness
ε = eddy viscosity defined by Eq. (8)
θ_shock = shock angle
λ = outer law mixing-length constant, 0.090
μ = laminar (molecular) viscosity
ξ = transformed x-coordinate, $\int_0^x \rho_e \mu_e U_e\, dx$
ρ' = fluctuating mass density
$\bar{\rho}$ = mean mass density
ρ_e = mass density at outer edge of boundary layer
ρ_∞ = freestream mass density
χ = crossflow Reynolds number defined by Eq. (14)

Superscripts

$'$ = fluctuating quantity
$\bar{}$ = averaged quantity with respect to time

Subscripts

e = outer edge of boundary layer
pc = phase-change paint
ref = reference
sl = streamline coordinates
w = wall
∞ = freestream

Presented as Paper 73-637 at the AIAA 6th Fluid and Plasma Dynamics Conference, Palm Springs, Calif., July 16–18, 1973; submitted August 21, 1973; revision received May 31, 1974. The research reported herein was sponsored by Arnold Engineering Development Center (AEDC), Air Force Systems Command. The work was performed by ARO, Inc., contract operator of AEDC. Further reproduction is authorized to satisfy needs of the U.S. government.

Index categories: Boundary Layers and Convective Heat Transfer—Laminar; Boundary Layers and Convective Heat Transfer—Turbulent; Boundary-Layer Stability and Transition.

* Supervisor, Project Support and Special Studies Section, Aerodynamics Projects Branch, von Kármán Gas Dynamics Facility. Associate Fellow AIAA.

† Project Engineer, Aerothermodynamics Section, Aerodynamics Projects Branch, von Kármán Gas Dynamics Facility. Member AIAA.

I. Introduction

THE prediction of the thermal environment to be encountered by vehicles during atmospheric entry requires extrapolation of ground test (wind-tunnel) data by appropriate theoretical methods. Ideally, this may be accomplished by ensuring that

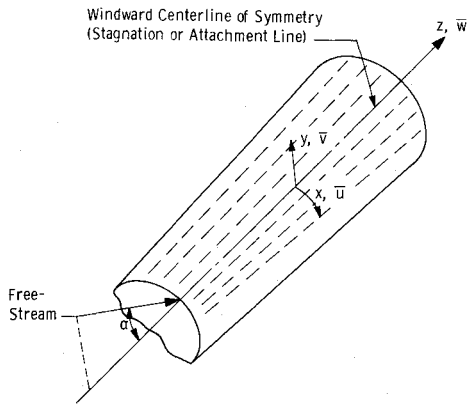

Fig. 1 Windward surface orthogonal coordinate system for general lifting body configurations at incidence.

ground test data, taken over appropriate ranges of Mach number and Reynolds number, can be calculated from theory and then extrapolated to flight by applying that theory to flight conditions. The concluding summary on p. 255 of Ref. 1 concerning the current status and future needs of flowfield analysis techniques for Space Shuttle applications states that "the need for a three-dimensional method applicable at high angles of attack is clear." The present paper documents one such technique applicable to the windward surface of general lifting body configurations at high angles of incidence under hypersonic perfect gas wind tunnel conditions with primary emphasis placed on development of an engineering-type analysis which is accurate and easy to use. Complete documentation of the present analysis technique is given in the report by Adams and Martindale[2] which includes a source deck listing and sample input-output for the digital computer code.

II. Analysis

"Strip Theory" Approach

The basic aerodynamic concept applied in the present analysis is termed "strip theory" in the sense defined by Sec. 7 in Chap. 1 of the book by Hayes and Probstein.[3] The mathematical justification for "strip theory" may be found on pp. 103–112 and pp. 342–355 of Hayes and Probstein[3] in terms of generalized hypersonic small-disturbance theory. The most important feature of this approach as it relates to lifting bodies at high angle of attack in a hypersonic flow is that *the local flow depends only on the local cross-sectional shape and the local angle of attack.* Further, the local flow behavior is independent of flow behavior at other body locations under the restriction of body smoothness (no discontinuities in body cross sections), which is mathematically represented by the condition $\partial/\partial z = 0$ relative to the general lifting body geometry defined in Fig. 1.

As noted on p. 27 in Hayes and Probstein,[3] the previously defined "strip theory" is applicable to both inviscid and viscous flows. Hence, the "strip theory" approach applied locally results in a quasi-three-dimensional analysis similar to the classical cases of infinite yawed cylinder and infinite swept-wing flows which were well known and discussed in many references.[2]

Range of Applicability of the "Strip Theory" Approach

A concise summary of the applicability of the "strip theory" approach to general lifting body configurations may be stated as follows: "Strip theory applied to the windward surface of general lifting body configurations at high angles of incidence in a hypersonic flow may be expected to be applicable in the body areas free of external flow interference (such as shock interference) and where the body planform width varies slowly and smoothly. The angle of attack must be sufficiently large that the surface flow emanates from the stagnation line (centerline) of the body and flows smoothly outward in a downstream direction over the windward surface." Illustrations of how surface oil flow visualization photographs (taken under hypersonic wind tunnel conditions) can be used to discern applicability of the "strip theory" approach are given in Ref. 2.

Governing Boundary-Layer Equations

The present analysis employs the three-dimensional compressible turbulent boundary-layer equations in terms of time-averaged mean flow quantities as derived by Vaglio-Laurin.[4] Assuming the ratio of boundary-layer thickness to local surface curvature to be everywhere small, the governing equations of motion, in terms of the orthogonal coordinate system x, y, z illustrated in Fig. 1, reduce to the following.

Continuity

$$\frac{\partial \bar{\rho}\bar{u}}{\partial x} + \frac{\partial \bar{\rho}\bar{V}}{\partial y} + \cancelto{0}{\frac{\partial \bar{\rho}\bar{w}}{\partial z}} = 0 \tag{1}$$

x-Momentum

$$\bar{\rho}\bar{u}\frac{\partial \bar{u}}{\partial x} + \bar{\rho}\bar{V}\frac{\partial \bar{u}}{\partial y} + \bar{\rho}\bar{w}\cancelto{0}{\frac{\partial \bar{u}}{\partial z}} = -\frac{\partial \bar{p}}{\partial x} + \frac{\partial}{\partial y}\left[(\mu+\varepsilon)\frac{\partial \bar{u}}{\partial y}\right] \tag{2}$$

y-Momentum

$$\partial \bar{p}/\partial y = 0 \tag{3}$$

z-Momentum

$$\bar{\rho}\bar{u}\frac{\partial \bar{w}}{\partial x} + \bar{\rho}\bar{V}\frac{\partial \bar{w}}{\partial y} + \bar{\rho}\bar{w}\cancelto{0}{\frac{\partial \bar{w}}{\partial z}} = -\cancelto{0}{\frac{\partial \bar{p}}{\partial z}} + \frac{\partial}{\partial y}\left[(\mu+\varepsilon)\frac{\partial \bar{w}}{\partial y}\right] \tag{4}$$

Energy

$$\bar{\rho}\bar{u}\frac{\partial \bar{H}}{\partial x} + \bar{\rho}\bar{V}\frac{\partial \bar{H}}{\partial y} + \bar{\rho}\bar{w}\cancelto{0}{\frac{\partial \bar{H}}{\partial z}} = \frac{\partial}{\partial y}\left\{\frac{\mu}{Pr}\left(1+\frac{\varepsilon}{\mu}\frac{Pr}{Pr_t}\right)\frac{\partial \bar{H}}{\partial y} + \mu\left[\frac{Pr-1}{Pr} + \frac{\varepsilon}{\mu}\frac{Pr_t-1}{Pr_t}\right]\left[\bar{u}\frac{\partial \bar{u}}{\partial y} + \bar{w}\frac{\partial \bar{w}}{\partial y}\right]\right\} \tag{5}$$

where

$$V = \bar{v} + (\overline{\rho' v'}/\bar{\rho}) \tag{6}$$

$$\bar{H} = \bar{h} + (\bar{u}^2 + \bar{w}^2)/2 \tag{7}$$

Implicit in the abovementioned equations is the requirement of an infinite extent body of the yawed cylinder or yawed wing type, which leads to the term $\partial/\partial z = 0$ as discussed in the first part of the current section. The Reynolds stress or turbulent shear terms in the momentum Eqs. (2) and (4) and the turbulent flux of total enthalpy in the energy Eq. (5) have been modeled via a scalar eddy viscosity-turbulent Prandtl number approach which will be described later in this section.

The associated boundary conditions on the previously defined equations are no slip and no mass transfer at the wall, as well as a prescribed constant wall enthalpy. The y-momentum equation (3) reveals that the static pressure variation across the boundary layer is negligible, and hence the static pressure, $\bar{p}(x)$, is regarded as an external input to the boundary-layer analysis from a separate inviscid analysis. The outer edge velocities, U_e and W_e, as well as the outer-edge static enthalpy, h_e, must be determined from the inviscid analysis consistent with the imposed static-pressure distribution.

Gas Model

The gas model used in the present study restricted to hypersonic wind tunnel conditions is thermally and calorically perfect air or nitrogen. The laminar viscosity is taken to obey Sutherland's law while the laminar Prandtl number is assumed to have a constant value of 0.71 across the entire boundary layer for both air and nitrogen.

Turbulent Transport Model

The approach used in the present analysis is to model the Reynolds stress or turbulent shear terms in the momentum equations and the turbulent flux of total enthalpy in the energy equation as functions of the mean-flow variables following Adams,[5-7] whose studies are based on the analysis by Hunt, Bushnell, and Beckwith.[8] The Prandtl mixing-length hypothesis is applied in conjunction with the assumption that the eddy viscosity is a *scalar function independent of coordinate direction* (which means physically that the turbulent shear stress acts in the mean rate of strain direction) so as to result in an eddy viscosity relationship of the form

$$\varepsilon = \bar{\rho} l_*^2 (\partial \bar{G}/\partial y) \tag{8}$$

where $\bar{G}$ is a scalar velocity function defined by

$$\frac{\partial \bar{G}}{\partial y} = \left[\left(\frac{\partial \bar{u}}{\partial y} \right)^2 + \left(\frac{\partial \bar{w}}{\partial y} \right)^2 \right]^{1/2} \tag{9}$$

The two-layer (inner-outer) variation of the mixing length, l_*, is taken from the boundary-layer analysis by Patankar and Spalding[9]

$$\left.\begin{aligned} l_* &= k_* y, \quad \text{for} \quad 0 < y \leqq \lambda y_l/k_* \\ l_* &= \lambda y_l, \quad \text{for} \quad \lambda y_l/k_* < y \end{aligned}\right\} \tag{10}$$

where the values for the various numerical constants are taken to be $k_* = 0.435$ and $\lambda = 0.09$. The value of y at the point where the velocity in the boundary layer is equal to 0.99 of the velocity at the boundary-layer outer edge is used to define the distance y_l. The so-called van Driest exponential damping[10] is applied for the near wall region in conjunction with the suggestion by Patankar and Spalding[9] that the *local* value of the *total* shear stress be used instead of the wall value originally recommended by van Driest.

The total heat flux expression may be written in the form

$$\dot{q} = \mu \left[\frac{1}{Pr} + \frac{\varepsilon}{\mu} \frac{1}{Pr_t} \right] \frac{\partial \bar{h}}{\partial y} \tag{11}$$

For the present work, the turbulent Prandtl number is taken to remain constant at the value 0.90 across the entire boundary layer as recommended by Patankar and Spalding.[9]

For the case of purely laminar flow in the present analysis, the eddy viscosity is set identically equal to zero so that the governing turbulent boundary-layer equations reduce to their laminar counterpart.

Numerical Solution of the Governing Boundary-Layer Equations

The governing boundary-layer equations are transformed to Illingworth-Levy variables which allow linearized finite-difference equivalents of the equations to be easily formulated. These are then solved using an iterative, marching, implicit finite-difference integration technique involving inversion of tri-diagonal matrices. Full details of this numerical approach are given in Appendix III of Ref. 2.

Inviscid Flowfield

The inviscid flowfield quantities needed for input to the present boundary-layer analysis (such as U_e, W_e, $\bar{p}$, etc.) are determined in a simplified manner consistent with the "strip theory" principle. Stagnation or attachment line ($x = 0$) parameters are used in conjunction with an analysis of a *local* cross-sectional body cut in a plane *normal* to the stagnation or attachment line axis (which is the z-axis shown in Fig. 1).

The present windward surface inviscid parameters along the centerline of Space Shuttle orbiter configurations are calculated from tangent-cone theory applied *locally*. Variable entropy solutions for blunt-nosed configurations (see Ref. 11, for example) indicate that this is valid at surface distances greater than about 20 nose radii for the conditions currently considered. The particular form of tangent-cone theory applied in the present analysis is based on a simple approximate solution for the hypersonic small-disturbance form of the Van Dyke stream-function equation[12] as developed by Rasmussen.[13]

The present analysis utilizes the one-strip method of integral relations digital computer code developed by South[14] to calculate the x-direction surface pressure distribution over a body cross-sectional cut in a plane normal to the z-axis. The inviscid cross-flow velocity, $U_e(x)$, distribution is determined from

$$\rho_e U_e (dU_e/dx) + d\bar{p}/dx = 0 \tag{12}$$

At the stagnation or attachment line ($x = 0$), the limiting form of Eq. (12) reduces to

$$\left[\frac{dU_e}{dx} \right]_{x=0} = \left\{ \left[\frac{-1}{\rho_e} \frac{d^2\bar{p}}{dx^2} \right]_{x=0} \right\}^{1/2} \tag{13}$$

The term ρ_e is evaluated using the inviscid conical flow approach described above. The derivative term $d^2\bar{p}/dx^2$ is evaluated via numerical differentiation of the pressure distribution obtained from the South one-strip method of integral relations. Complete detail of the special procedures for determination of the sonic point location, either natural or forced, is given in Sec. 2.10.3 of Ref. 2.

Boundary-Layer Transition Correlation Parameter

A type of (three-dimensional) boundary-layer transition which has received little attention to date relative to Space Shuttle-type configurations is the so-called crossflow-induced transition first observed by Owen and Randall[15] and Chapman[16] in swept-wing and yawed cylinder flows. A general discussion of the basic phenomenon and its three-dimensional nature may be found in the recent report by Adams.[17] Briefly, three-dimensional cross-flow has an adverse effect on laminar boundary-layer stability in that a system of streamwise vortices contained within the boundary layer may be formed, apparently because of the inflection point in the rotated crossflow velocity profile illustrated in Fig. 2 which is unstable to small disturbances.

The abrupt formation of these vortices and also the development of complete turbulence, i.e., transition, in a three-dimensional boundary layer can apparently be correlated with a so-called maximum local crossflow Reynolds number, χ, defined as[15-17]

$$\chi = \frac{\rho_e \bar{w}_{sl,\max} \delta}{\mu_e} \tag{14}$$

where $\bar{w}_{sl,\max}$ is the maximum crossflow velocity in the streamline coordinates of Fig. 2, and δ is the boundary-layer thickness; ρ_e and μ_e are the values of density and viscosity, respectively, evaluated at the inviscid edge conditions. Owen and Randall[15] found the critical value of crossflow Reynolds number for vortex formation and for crossflow-induced transition to be 125 and 175, respectively, based on the leading edge of swept wings at subsonic speeds. The work by Chapman[16] on swept cylinders at supersonic speeds (freestream Mach numbers up to 7) indicates that

$\chi < 100$ laminar boundary layer

$100 \leqq \chi \leqq 200$ vortex formation and transitional boundary layer

$\chi > 200$ turbulent boundary layer

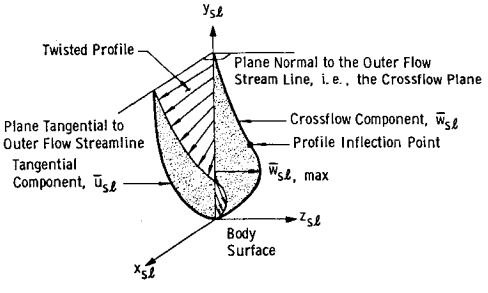

Fig. 2 Three-dimensional boundary-layer velocity profiles in streamline coordinates.

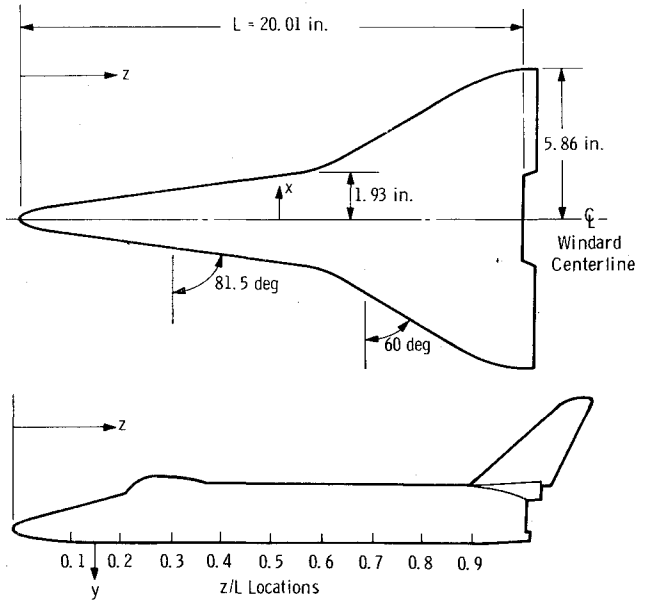

Fig. 3 North American Rockwell (NAR) delta wing orbiter configuration 161B (0.009-scale).

which means that the crossflow stability criterion of Owen and Randall may apparently be expected to apply without change on cylindrical leading edges for both subsonic and supersonic flows. Chapman's work further showed that the amount of crossflow needed to induce crossflow instability downstream of the leading edge was very small—on the order of 1–5% of the inviscid edge velocity for the conditions observed. This means physically that on Space Shuttle configurations at high angles of incidence with large spanwise pressure gradients, off-centerline boundary-layer transition may more likely be caused by instability of the crossflow than by instability of the streamwise velocity profile (i.e., Tollmien-Schlichting instability) because of the extremely small amount of crossflow needed to cause transition at small values of the local crossflow Reynolds number.

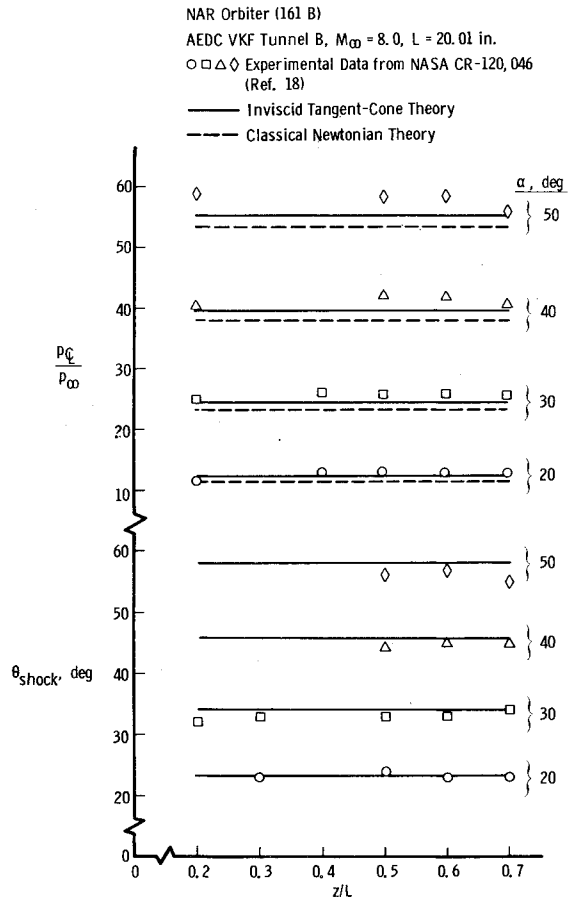

Fig. 4 Centerline pressure and shock angle distribution on the NAR orbiter at incidence.

III. Results and Discussion

North American Rockwell (NAR) Delta Wing Orbiter Configuration 161B

One of the Phase B Space Shuttle designs tested extensively in the AEDC-VKF Hypersonic Wind Tunnel (B) at Mach 8 was the North American (NAR) Delta Wing Orbiter Configuration 161B (0.009 scale). A side and windward planform view of this configuration is shown in Fig. 3; more complete details of the body geometry can be found in Refs. 18–20, which document the data taken during the AEDC wind tunnel tests. The NAR Orbiter Configuration 161B windward surface cross-sectional shapes can be well represented in the axial coordinate range $0.1 < z/L < 0.5$ by a flatfaced body with rounded shoulders having a natural sonic point; between $z/L = 0.5$ and $z/L = 0.7$, a flatfaced body with rounded shoulders approximation having a forced sonic point at the leading edge appears reasonable. For $z/L > 0.7$ the delta wing is sweeping out from the body and the "strip theory" approach of the present analysis is not applicable.

The top portion of Fig. 4 shows a comparison of both inviscid tangent-cone and classical Newtonian theories relative to the experimental centerline pressure measurements of Ref. 18 on the NAR Orbiter Configuration 161B in the angle-of-attack range $20° \leqq \alpha \leqq 50°$ under Mach 8 hypersonic flow conditions. At the lower angles of attack, inviscid tangent-cone theory is in good agreement with the experimental data. At the highest angle of attack (50°), the experimental measurements are approximately 5% above the inviscid tangent-cone theory and about 10% above classical Newtonian theory. As shown in the bottom portion of Fig. 4, inviscid tangent-cone theory is also adequate for estimation of windward centerline shock angles on the present NAR configuration in the angle-of-attack range from 20° to 50°.

To calculate heating rate distributions on the NAR configurations, body cross-sectional cuts were made at $z/L = 0.3$, 0.5, and

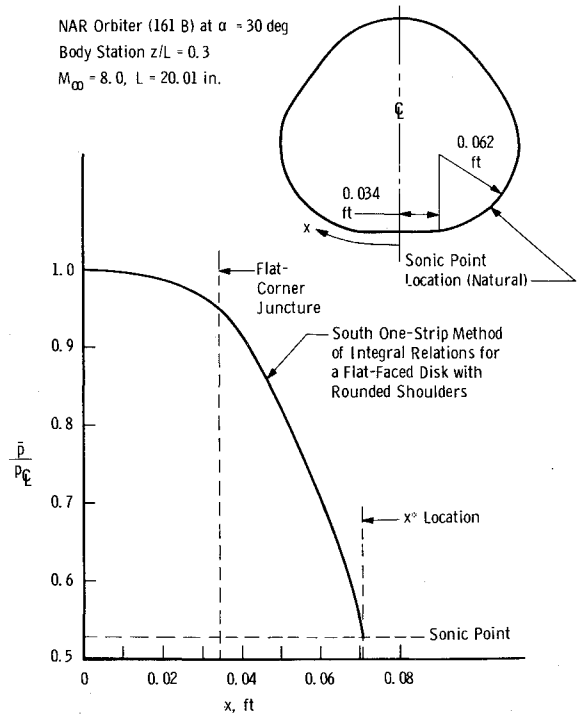

Fig. 5 Spanwise pressure distribution on the NAR orbiter at incidence.

0.7, and the spanwise pressure distribution at these locations was determined via the inviscid method of Sec. II. Figure 5 shows the results of this approach for the body station $z/L = 0.3$ on the NAR Orbiter Configuration 161B at 30° angle of attack in a Mach 8 hypersonic flow. Note from Fig. 5 that the windward cross-sectional shape has been approximated by a flatfaced body with rounded corners having a natural sonic point location, i.e., a flatfaced disk with rounded shoulders. It should be noted that the spanwise pressure distributions at $z/L = 0.3$ for both the 40° and 50° angle-of-attack cases are almost identical with the 30° case of Fig. 5.

Heating rate distributions calculated from the present three-dimensional laminar and turbulent boundary-layer analysis are presented in Figs. 6 and 7 relative to the experimental measurements of Ref. 19 for the NAR Orbiter Configuration 161B. Figure 6 gives the windward centerline Stanton number distributions for both laminar and turbulent boundary layers at 30° angle of attack under AEDC-VKF Tunnel B high Reynolds number conditions. The turbulent data (shown as closed or darkened symbols) were obtained using carborundum grit placed on the windward surface to "trip" the boundary layer; the laminar and transitional data (shown as open symbols) were obtained on a smooth-surface model. A discussion of the carborundum grit "tripping" technique is given in Ref. 19. All of the experimental heat-transfer data of Ref. 19 were taken using the thin-skin thermocouple technique under relatively cold-wall ($T_w/T_{0,\infty} \approx 0.4$) conditions. The calculations were performed for the $z/L = 0.3$, 0.5, and 0.7 stations discussed in the previous paragraph, and the theoretical lines shown in Fig. 6 are fairings through the three calculated values. In general, good to excellent agreement between theory and experiment is observed for both the laminar and turbulent heat-transfer distributions along the windward centerline at 30° angle of attack; results presented in Ref. 2 reveal good agreement for the 40° and 50° angle-of-attack conditions as well.

The spanwise Stanton number distributions for both laminar and turbulent boundary layers at the body station location $z/L = 0.3$ on the NAR Orbiter Configuration 161B at 30° and 50° angles of attack under AEDC-VKF Tunnel B high Reynolds number conditions are given in Fig. 7. Note that this body location corresponds to the spanwise pressure distribution of Fig. 5 discussed previously. As can be seen from Fig. 7, good to excellent agreement between the present three-dimensional

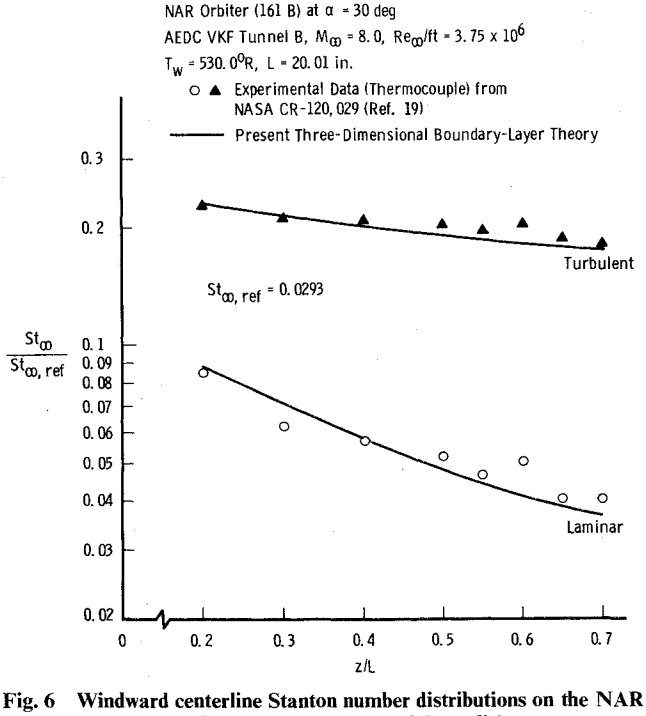

Fig. 6 Windward centerline Stanton number distributions on the NAR orbiter under AEDC-VKF Tunnel B conditions.

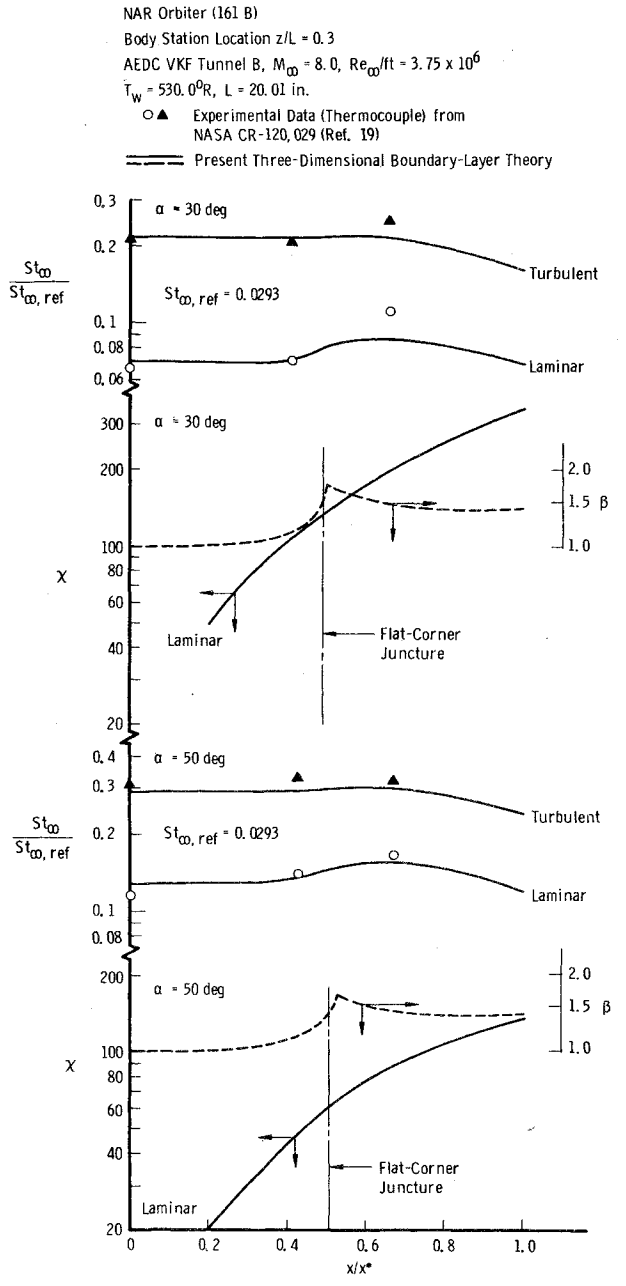

Fig. 7 Spanwise Stanton number, crossflow Reynolds number, and inviscid velocity gradient parameter distributions on the NAR orbiter under AEDC-VKF Tunnel B conditions.

boundary-layer theory and the experimental measurements of Ref. 19 is observed for the case of a fully turbulent boundary layer at both angle-of-attack conditions. In addition, the agreement between the present three-dimensional laminar boundary-layer theory and experiment is excellent for the 50° angle-of-attack case. For the 30° angle-of-attack condition, the laminar theory is in good agreement with experiment on the body centerline and at the spanwise location $x/x^* \approx 0.4$; at $x/x^* \approx 0.65$ the measured heat-transfer rate is some 15–25% greater than the corresponding calculated laminar value. Reference to the bottom portion of Fig. 7 shows that the crossflow Reynolds number, χ, is in the range $100 < \chi < 200$ at the spanwise location $x/x^* \approx 0.65$ for the 30° angle-of-attack condition; $\chi \approx 90$ for the 50° angle-of-attack case. Hence, the boundary layer at the spanwise location $x/x^* > 0.65$ for the 30° angle-of-attack condition may be in a transitional state because of three-dimensional crossflow-dominated laminar boundary-layer instability.

The χ criterion of Sec. II suggests that the boundary layer should be in a fully turbulent state for $\chi > 200$. Such is

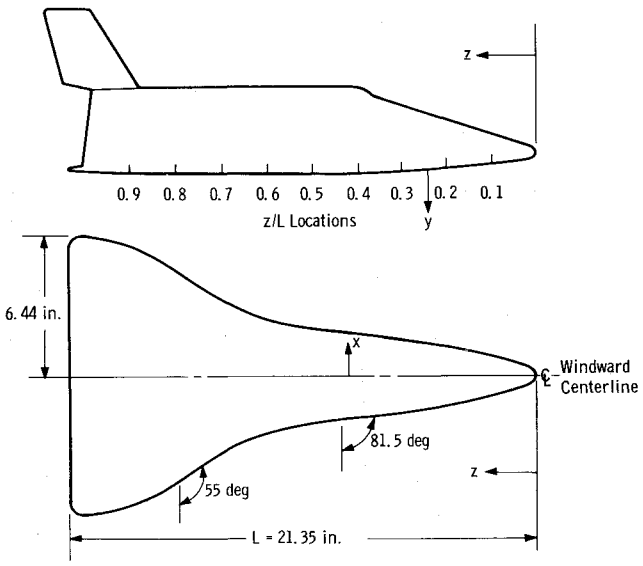

Fig. 8 McDonnell-Douglas (MDAC) delta wing orbiter configuration (0.011-scale).

obviously not the case in Fig. 7. To understand why a fully turbulent condition is not attained, examine the inviscid velocity gradient parameter β distribution as shown in the bottom portion of Fig. 7 along with the χ curve. As can be seen, the boundary layer is being substantially accelerated at the spanwise station of interest, $x/x^* \approx 0.65$. Hence, it appears reasonable to postulate that the present three-dimensional flow tends to promote laminar boundary-layer instability and transition at the same time that the flow acceleration tends to stabilize the boundary layer.

McDonnell-Douglas (MDAC) Delta Wing Orbiter Configuration

The only Phase B Space Shuttle design tested extensively in both the AEDC-VKF Hypersonic Wind Tunnel (B) at Mach 8 and the AEDC-VKF Hypervelocity Wind Tunnel (F) at nominal Mach number 10.5 was the McDonnell-Douglas (MDAC) Delta Wing Orbiter configuration (0.011 scale). Side and windward planform views of this configuration are shown in Fig. 8; more complete details of the body geometry can be found in Refs. 21 and 22, which document the data taken during the AEDC wind-tunnel tests. The MDAC Orbiter configuration windward surface cross-sectional shapes can be well represented in the axial coordinate range $0.1 < z/L < 0.4$ by a swung-arc body having a forced sonic point at the leading edge; between $z/L = 0.4$ and $z/L = 0.7$, the aft delta wing is sweeping out from the body and the "strip theory" approach of the present analysis is not applicable.

A comparison of both calculated and experimental results for windward centerline Stanton number distributions on the MDAC Orbiter configuration at 50° angle of attack under both AEDC-VKF Tunnel B and F conditions is given in Fig. 9. In general, the present three-dimensional fully turbulent boundary-layer calculations are in good agreement with the experimental results from both tunnels.

The effects of change in the freestream Reynolds number at an essentially common freestream Mach number and wall temperature ratio can be seen from the two AEDC-VKF Tunnel F time point results on Fig. 9. Note from the top part of Fig. 9 that the freestream Reynolds number decreases by approximately a factor of three between the 61 and 135 msec time points. As shown by Widhopf,[23] the turbulent heat-transfer formulation derived by Vaglio-Laurin[4] based on inviscid streamline spreading for bodies at incidence in a hypersonic flow in conjunction with a laminar sphere stagnation point reference value computed from the Fay and Riddell theory[24] leads to a freestream Reynolds number effect on the turbulent heat-transfer rate in the form [see Eq. (6) of Ref. 23]

$$\frac{\dot{q}_{\text{Turbulent}}}{\dot{q}_{\text{Laminar}}} \propto [Re_{\infty,L}]^{3/10} \tag{15}$$

That this $\frac{3}{10}$-power dependence of the freestream Reynolds number on turbulent heat-transfer rate is also applicable to lifting body configurations at high angles of incidence can be seen upon careful examination of the calculated and experimental results for the two AEDC-VKF Tunnel F time points in Fig. 9.

Verification of the wall temperature effect on turbulent boundary-layer heat transfer as reflected in the Stanton number may be seen in Fig. 9 by comparison of the AEDC-VKF

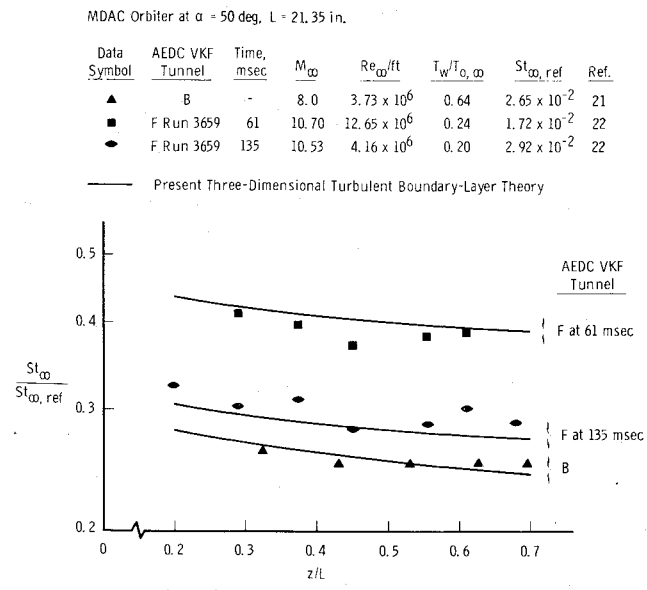

Fig. 9 Effects of Mach number, Reynolds number, and wall temperature ratio on MDAC orbiter windward centerline turbulent heat transfer under high angle-of-attack conditions.

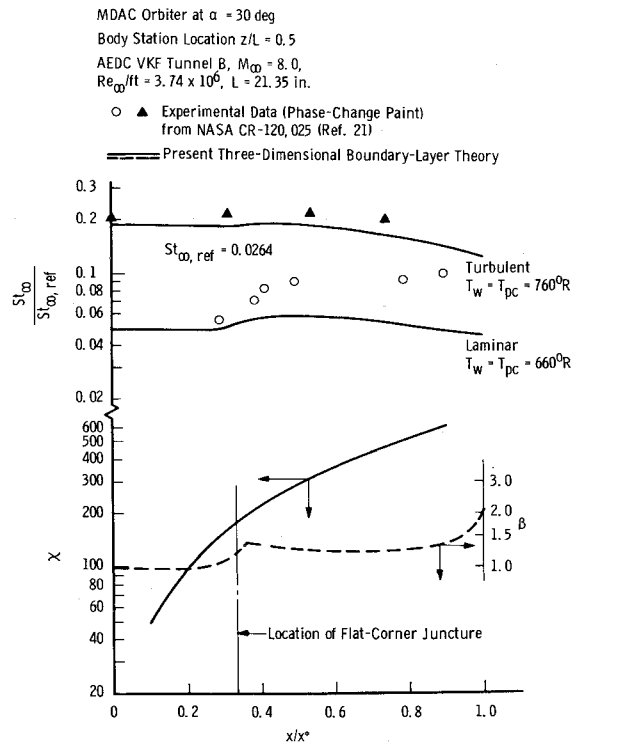

Fig. 10 Spanwise Stanton number, crossflow Reynolds number, and inviscid velocity gradient parameter distributions on the MDAC orbiter under AEDC-VKF Tunnel B conditions.

Tunnel B and Tunnel F at 135 msec results. Note that the freestream unit Reynolds number is about the same for these two flows with a slightly unmatched freestream Mach number; wall temperature ratio is the primary difference ($T_w/T_{0,\infty} = 0.64$ in B and 0.20 in F). Agreement between the present calculations and experiment is excellent, verifying that the current analysis does indeed yield valid estimates of wall temperature effects on the three-dimensional turbulent boundary layer under hypersonic conditions.

The spanwise Stanton number distributions for both laminar and turbulent boundary layers at the body station location $z/L = 0.5$ on the MDAC Orbiter configuration at 30° angle of attack under AEDC-VKF Tunnel B high Reynolds number conditions are given in Fig. 10. The experimental data shown on Fig. 10 were determined by the phase-change paint technique employing Stycast® models using Tempilaq® as the surface temperature indicator. Full details of the experimental results including the AEDC-VKF phase-change paint data reduction technique are given in Ref. 21. The turbulent data (shown as closed or darkened symbols) were obtained using carborundum grit placed on the windward surface to "trip" the boundary layer; the laminar and transitional data (shown as open symbols) were obtained on a smooth-surface model. A discussion of the carborundum grit "tripping" technique is given in Ref. 21.

As can be seen from Fig. 10, good to excellent agreement between the present three-dimensional boundary-layer theory and the experimental measurements of Ref. 21 is observed for the case of a fully turbulent boundary layer. The key point of interest in Fig. 10 is the clear indication of boundary-layer transition beginning at a spanwise location where the crossflow Reynolds number, χ, reaches a value of approximately 100. The present MDAC Orbiter results are in direct agreement with the crossflow transition results for the NAR Orbiter Configuration 161B under identical hypersonic, high Reynolds number conditions so that all previous comments, discussion, and conclusions regarding crossflow transition, as well as flow acceleration effects, apply without change to the present case. The 30° angle-of-attack condition of Fig. 10 indicates that crossflow transition to a turbulent boundary layer may be completed near the sonic point location, while at and near the centerline the boundary layer remains in a laminar state.

Conclusions

Comparisons of the present "strip theory" approach with hypersonic wind tunnel data on two Phase B Space Shuttle configurations have been presented to establish and ascertain the basic validity and applicability of the current technique. Under conditions where the basic requirements for applicability of "strip theory" are satisfied, the present analytical approach yielded accurate estimates of wall measurable flow parameters (surface pressure and surface heat transfer) for both configurations considered. One of the more important results of the current study was the tentative identification of spanwise crossflow-induced boundary-layer transition on Space Shuttle configurations at high incidence angles. Other significant findings include the $\frac{3}{10}$-power scaling of turbulent boundary-layer heat-transfer rate with respect to changes in the freestream Reynolds number, as well as wall temperature influence on turbulent boundary-layer heat transfer. Much more work remains to be done in the relatively unexplored area of crossflow-dominated boundary-layer transition coupled with flow acceleration effects before this phenomenon will be fully understood. The possibility of suitably designing the body cross-sectional contour to keep the crossflow Reynolds number at as small a value as possible deserves future attention.

References

[1] "Space Shuttle Aerothermodynamics Technology Conference, Vol. I—Flow Fields," TM X-2506, Feb. 1972, NASA.

[2] Adams, J. C., Jr. and Martindale, W. R., "Hypersonic Lifting Body Windward Surface Flow-Field Analysis for High Angles of Incidence," AEDC-TR-73-2, Feb. 1973, Arnold Engineering Development Center, Arnold Air Force Station, Tenn.

[3] Hayes, W. D. and Probstein, R. F., *Hypersonic Flow Theory*, 2nd ed., Vol. 1, Academic Press, New York, 1966.

[4] Vaglio-Laurin, R., "Turbulent Heat Transfer on Blunt-Nosed Bodies in Two-Dimensional and General Three-Dimensional Hypersonic Flow," *Journal of Aeronautical Sciences*, Vol. 27, No. 1, Jan. 1960, pp. 27–36.

[5] Adams, J. C., Jr., "Implicit Finite-Difference Analysis of Compressible Laminar, Transitional, and Turbulent Boundary Layers along the Windward Streamline of a Sharp Cone at Incidence," AEDC-TR-71-235, Dec. 1971, Arnold Engineering Development Center, Arnold Air Force Station, Tenn.

[6] Adams, J. C., Jr., "Finite-Difference Analysis of the Three-Dimensional Compressible Turbulent Boundary Layer on a Sharp Cone at Angle of Attack in a Supersonic Flow," AIAA Paper 72-186, San Diego, Calif., 1972.

[7] Adams, J. C., Jr., "Analysis of the Three-Dimensional Compressible Turbulent Boundary Layer on a Sharp Cone at Incidence in Supersonic and Hypersonic Flow," AEDC-TR-72-66, June 1972, Arnold Engineering Development Center, Arnold Air Force Station, Tenn.

[8] Hunt, J. L., Bushnell, D. M., and Beckwith, I. E., "The Compressible Turbulent Boundary Layer on a Blunt Swept Slab with and without Leading-Edge Blowing," TN D-6203, March 1971, NASA.

[9] Patankar, S. V. and Spalding, D. B., *Heat and Mass Transfer in Boundary Layers*, CRC Press, Cleveland, Ohio, 1968.

[10] van Driest, E. R., "On Turbulent Flow Near a Wall," *Journal of Aeronautical Sciences*, Vol. 23, No. 11, Nov. 1956, pp. 1007–1011, 1036.

[11] Johnson, C. B., "Boundary-Layer Transition and Heating Criteria Applicable to Space Shuttle Configurations from Flight and Ground Tests," TM X-2272, April 1971, NASA, pp. 97–156.

[12] Van Dyke, M. D., "A Study of Hypersonic Small-Disturbance Theory," Rept. 1194, 1954, NACA.

[13] Rasmussen, M. L., "On Hypersonic Flow Past an Unyawed Cone," *AIAA Journal*, Vol. 5, No. 8, Aug. 1967, pp. 1495–1497.

[14] South, J. C., Jr., "Calculation of Axisymmetric Supersonic Flow Past Blunt Bodies with Sonic Corners, Including a Program Description and Listing," TN D-4563, May 1968, NASA.

[15] Owen, P. R. and Randall, D. G., "Boundary Layer Transition on a Sweptback Wing," RAE TM Aero 277, May 1952, Royal Aircraft Establishment, Farnborough, England.

[16] Chapman, G. T., "Some Effects of Leading-Edge Sweep on Boundary Layer Transition at Supersonic Speeds," TN D-1075, Sept. 1961, NASA.

[17] Adams, J. C., Jr., "Three-Dimensional Laminar Boundary-Layer Analysis of Upwash Patterns and Entrained Vortex Formation on Sharp Cones at Angle of Attack," AEDC-TR-71-215, Dec. 1971, Arnold Engineering Development Center, Arnold Air Force Station, Tenn.

[18] Matthews, R. K., Martindale, W. R., and Warmbrod, J. D., "Surface Pressure and Inviscid Flow Field Properties of the North American Rockwell Delta-Wing Orbiter for Nominal Mach Number of 8," CR-120, 046, March 1972, NASA.

[19] Warmbrod, J. D., Martindale, W. R., and Matthews, R. K., "Heat Transfer Rate Measurements on North American Rockwell Orbiter (161B) at Nominal Mach Number of 8," CR-120, 029, Dec. 1971. NASA.

[20] Martindale, W. R., Matthews, R. K., and Trimmer, L. L., "Heat-Transfer and Flow-Field Tests of the North American Rockwell/General Dynamics Convair Space Shuttle Configurations," AEDC-TR-72-169, Jan. 1973, Arnold Engineering Development Center, Arnold Air Force Station, Tenn.

[21] Matthews, R. K., Martindale, W. R., and Warmbrod, J. D., "Heat Transfer Rate Distributions on McDonnell-Douglas Delta Wing Orbiter Determined by Phase-Change Paint Technique for Nominal Mach Number of 8," CR-120, 025, revised July 1972, NASA.

[22] Eaves, R. H., Buchanan, T. D., and Warmbrod, J. D., "Heat Transfer Investigation of the McDonnell-Douglas Delta Wing Orbiter at a Nominal Mach Number of 10.5," CR-120, 024, May 1972, NASA.

[23] Widhopf, G. F., "Heat Transfer Correlations for Blunt Cones at Angle of Attack," TR-0172 (S2816-63)-1, July 1971, Aerospace Corp., El Segundo, Calif.

[24] Fay, J. A. and Riddell, F. R., "Theory of Stagnation Point Heat Transfer in Dissociated Air," *Journal of Aeronautical Sciences*, Vol. 25, No. 2, Feb. 1958, pp. 73–85, 121.